Received: 7 December 2020 | Revised: 28 January 2021 | Accepted: 5 February 2021

DOI: 10.1002/ese3.882

RESEARCH ARTICLE

Energy Science & Engineering Open Access

Study on characteristics of particulate emission of diesel aftertreatment with reciprocating flow

Yangbo Deng[1] | **Xiaolong Wang**[2] | **Rongrui Li**[2] | **Zhitao Han**[2] | **Hongwei Wu**[3] | **Jingming Dong**[2] | **Wenbin Cui**[2] | **Yang Guo**[2]

[1]Naval Architecture and Ocean Engineering College, Dalian Maritime University, Dalian, China

[2]Maine Engineering College, Dalian Maritime University, Dalian, China

[3]Shool of Engineering and Computer Science, University of Hertfordshire, Hatfield, UK

Correspondence
Yangbo Deng, Naval Architecture and Ocean Engineering College, Dalian Maritime University, Dalian Linghai Road No. 1, Dalian, China
Email: dengyb@dlmu.edu.cn

Funding information
Coal Joint Fund of the National Natural Science Fund Committee of China—Shenhua Group Corporation Ltd., Grant/Award Number: U1361111; National Natural Science Foundation of China, Grant/Award Number: 5197022; Natural Science Foundation of Liaoning Province, China, Grant/Award Number: 2019-ZD-0164; Dalian Science and Technology Innovation Fund, Grant/Award Number: 2020JJ26SN065; Fundamental Research Funds for the Central Universities of China, Grant/Award Number: 3132019331

Abstract

In this article, in order to optimize diesel aftertreatment system with periodically reciprocating flow (PRF), an experimental study is conducted to investigate its characteristics such as pollution emissions, regeneration of diesel particulate filter (DPF), concentration, and size distribution of particulate matter (PM) escaped as well as temperature distribution under unidirectional flow and PRF operating conditions. The effects of reciprocating flow cycle and exhaust gas flow on the performance of aftertreatment system are investigated in detail. The energy efficiency analysis of the aftertreatment system is also carried out. Experimental results show that (a) as the temperature is lower than the light-off threshold of combustible gas, the aftertreatment system cannot restrain the formation of second particles under the low-temperature condition of unidirectional flow; and (b) the aftertreatment system demonstrates excellent performance of trapping particles and filter regeneration as the symmetrical temperature distribution is formed. The PM filter efficiency α_{PM} is 92%, and the specific energy consumption β is 124% for symmetrical temperature distribution; (c) the increase in reciprocating flow cycle could lead to the shifting of the temperature profiles, and this would affect the particle size distribution; (d) a certain increase in exhaust gas flow from engine would have insignificant change for the temperature distribution; and (e) the critical energy efficiency η_c of the system could reach 96.61%.

KEYWORDS

diesel aftertreatment, diesel particulate filter, particulate emission, reciprocating flow, regeneration of diesel particulate filter

1 | INTRODUCTION

Reverse flow reactor (RFR) can regenerate the heat through periodically reciprocating flow (PRF), and it can be recognized as one of most effective ways to increase the thermal efficiency of chemical reactor. Since the concept of RFR was first introduced and utilized to purify by Cottrell in 1935, afterward, many efforts have been devoted to its theoretical and practical development.[1,2] Although RFR is not new in concept, it has still been widely applied in various industrial field in recent years, such as the oxidation of volatile organic compounds (VOC), oxidation of sulfur dioxide (SO_2), the synthesis of methanol, and others.[3-7]

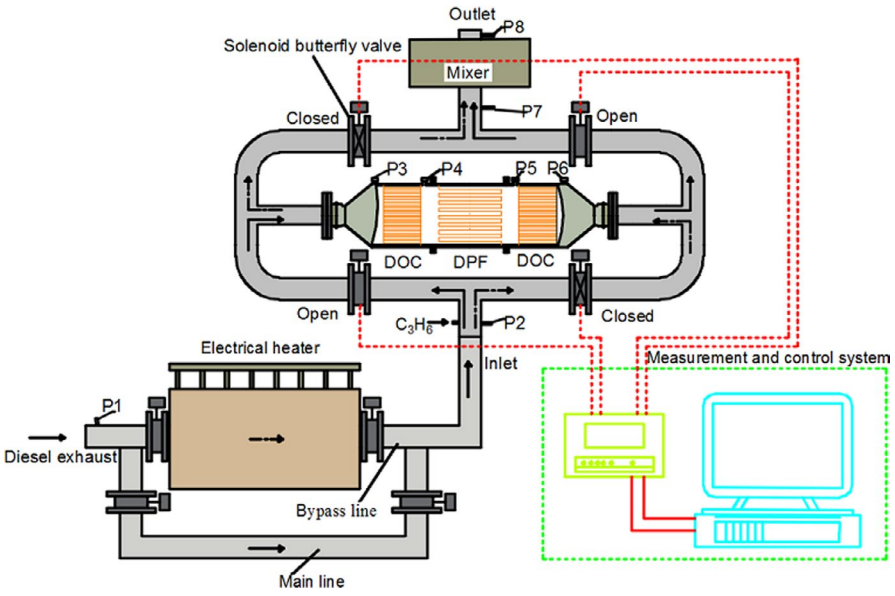

FIGURE 1 Schematic diagram of experimental apparatus

It is recognized that early scientists at Matros Technologies Inc, and Alternative Fuel Systems, Inc, applied the concept of RFR to remove pollutants from natural gas diesel engine and dual-fuel engine (DFE).[8,9] Their research work demonstrated that PRF could compensate for insufficient catalyst activity with the higher temperature achieved through regenerative heat exchange inside the catalyst monolith. And PRF could completely destruct the combustible components in the exhaust gas from DFE.[10] Afterward, they developed and tested a PRF aftertreatment device of DFE.[11] The conversion rates of reactive HC and CO are above 95%, and the conversion rates of CH_4 are around 90% when using the PRF aftertreatment device. In the meantime, the RFR technique was also used to facilitate the regeneration of diesel particulate filter (DPF) by Konstandopoulos and Kostoglou.[12] Their simulation results showed that PRF mechanism that could capture a high-temperature region in the DPF substrate could be capable of reducing the supplemental energy during regeneration process and thus to improve the overall thermal efficiency of the engine.[13]

Later on, Liu et al,[14,15] Zheng and Reader,[16] and Zheng et al[17] carries out a series of theoretical analysis and experimental study on the performance of PRF aftertreatment device. From investigation of PRF regeneration of DPF, Zheng et al[18] concluded that the temperature gradients could defer regeneration process and result in additional thermal stress. Therefore, they proposed a PRF aftertreatment structure that two inert monolith blocks were installed at the both ends of a DPF and analyzed the effect of two inert parts on device performance. Their results indicated that the inert monolith blocks could (a) enhance the heat recuperation, (b) reduce the temperature gradient, (c) decrease the substrate temperature, (d) increase the conversion efficiency of soot oxidation, and (e) decrease dependence on the thermal properties of the substrate materials and the operating conditions. Furthermore, Zheng et al[19-21] performed an experimental study on an aftertreatment system of diesel oxidation catalysts (DOCs) plus noncatalytic DPFs under PRF operations. Their results pointed out that the "light-off" temperature region could be maintained at certain locations. The critical energy efficiency could be improved with nonuniform supplemental energy distribution. Thus, it can be seen that the excellent performance of PRF aftertreatment mainly depends on the structure optimized of the device and the reasonable temperature distribution formed inside the device.

In order to further improve the performance of PRF aftertreatment, Deng et al[22] proposed a PRF aftertreatment system consisting of a catalyzed DPF and two DOCs. In their previous study on the operation performance of the aftertreatment system, they have validated its advantages that the mixed passive-active regeneration of DPF could be realized using a small amount of external fuel, the HC and CO escaped from upstream can also be oxidized in downstream DOC, and the ash accumulated in the filter could be blown away by reverse flow. These also further demonstrated that the PRF aftertreatment system was an ideal diesel aftertreatment system and a development goal of diesel aftertreatment technology. However, the PRF regeneration modes of DPF can also lead to low filtration efficiency, new or secondary particle escaped, and the nucleation of semivolatile particle because of the influence of reverse flow disturbance on particle deposited, the rapid oxidation of particles deposited, lower temperature at inlet and outlet, and the higher temperature in chemical reaction zone.

The significant increase in PM emission levels from DPF during regeneration compared with that of non-regeneration has caused many scholars' attention. A number of studies have been conducted to investigate the influence of regeneration conditions on the PM emission performance of DPF.[23-25] The various mechanisms obtained from these investigations

could reasonably explain the increase phenomenon of PM emission from DPF during regeneration.[26-30] But these past investigations main focused on the regeneration performance of traditional unidirectional flow DPF. In our current work, we will carry out study on the characteristics of the pollution emissions, the concentration and size distribution of PM emissions, the temperature distribution, and the energy efficiency of the PRF aftertreatment applied in high power diesel engine.

2 | EXPERIMENTAL APPARATUS AND METHODS

In the current study, a test rig for diesel aftertreatment system with PRF is set up. The test rig mainly consists of a PRF aftertreatment system, a diesel engine, exhaust pipelines, and measurement system, as shown in Figure 1.

2.1 | PRF aftertreatment system, diesel engine, and exhaust pipelines

PRF aftertreatment system is mainly composed of two DOCs, a DPF, flow pipelines, and a mixer. Two DOCs are arranged on both sides of the DPF, and a symmetrical structure of DOC+DPF+DOC is formed. The characteristics of DOCs and DPF have been described in detail in literature 22. In the current study, for the purpose of completeness, they are listed in Table 1. Two pairs of synchronously opening and closing valves in the flow pipelines are used to control the PRF of the aftertreatment system. The exhaust gas flows from right to left through the aftertreatment system is called the forward flow, whereas the flow from left to right is defined as the backward flow. A 30-L container is used as the mixer before the outlet. In the PRF experiment, the reciprocating flow cycle T_c is separately set at 50, 80, and 100 s. The P1-P8 measuring holes are arranged in the system and used to extract samples.

TABLE 1 Characteristics of DOCs and DPF

	DOC	DPF
Pore density/cpsi	300	200
Main material	Cordierite	Cordierite
Porosity/%	35-40	50-60
Wall thickness of channel/mm	0.25	0.3
Carrier average pore diameter/μm	3-7	8-20
Noble metal catalysts	Pt, Pd	Pt, Pd
Catalyst load/(g m^{-3})	706.2	353
Catalyst carriers	Al_2O_3 + Ce(Zr)O_2	Al_2O_3 + Ce(Zr)O_2
Length/mm	152.4	254
Diameter/mm	240	240

The diesel engine is a six-cylinder, turbo-charging, intercooling, and 110kW heavy-duty diesel engine. The diesel engine burns $0^{\#}$ diesel oil (National V emission standard) and is operated under idle conditions. The diesel engine runs in the ambient temperature of −10°C. During the experiment, the volume flow of exhaust gas q_v is, respectively, set at 260, 300, and 340 m^3/h through adjusting the throttle valve of the diesel engine.

The exhaust pipelines are set a bypass line with a 30 KW electrical heater. At the startup of the system, the bypass line is opened while the main line is closed. The electrical heater is used to heat the exhaust gas to the temperature starting the system. Meanwhile, a certain amount of propane gas is introduced at the inlet in order to initiate a thermal regeneration of DPF. As a reasonable temperature distribution in the system is established, the main line is opened and the bypass line is closed. During the experiment, 0.16 m^3/h of the propane gas is continually introduced at the inlet. When the temperatures periodically fluctuate and the fluctuating amplitude is nearly equal at a measuring position, the system is considered to be in quasisteady states.

2.2 | Measurement system

In Figure 2, the K-type thermocouples T2-T14 are separately located in two DOCs at intervals of about 30 mm and the DPF at intervals of about 42 mm to measure the temperature of the substrate along the centerline. Thermocouples T1 and T15 are placed at the outsides of two DOCs in order to measure the temperature of the exhaust gas. In the following analysis of temperature distribution, we have ignored the space between DOCs and DPF.

The flow rate of the exhaust gas will be measured using a vortex flow meter, and the flow rate of the propane gas will be measured using a glass rotameter. The pressures at P3 and P6 are measured with piezoresistive pressure transmitters. The concentrations of PM emission in the exhaust gas are measured using a SMG 100 Dust Measuring Device. The measuring range of particle diameters is from 0.1 to 10 μm using Dust Measuring Device. The components of gaseous pollutants in the exhaust gas are measured using a Testo 350 flue gas analyzer. In order to measure the average value of CO, PM, NO, and NO_2 components in exhaust gas under the PRF operation, the exhaust gas firstly flows through the mixer before the outlet. For different reciprocating flow cycles T_c, the average values of total mass concentration of particulates and gas components are calculated from the

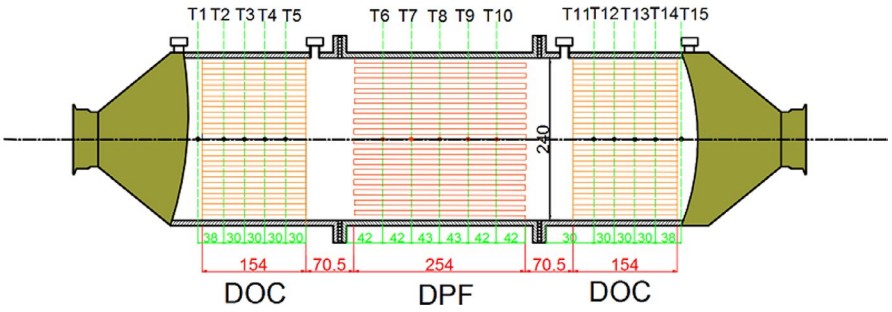

FIGURE 2 Schematic diagram of thermocouple arrangement

parameters continuously measured in 30 T_c as the system is under quasisteady-state conditions.

The size distributions of PM are measured using sequential mobility particle sizer and counter (SMPS+C) system. The exhaust gas will be firstly extracted into a dilution device from measuring hole and is diluted with ambient air to a dilution ratio of 80 before introduced into SMPS+C system. According to literatures 31 and 32, if the total dilution ratio is higher than 60, particle agglomeration should be remarkably reduced and the measuring results will be close to the practical situation. The sampling pipe of SMPS+C system connects to the dilution device, the sampling aerosol flow is at 0.3 lpm, the sheath airflow is at 3 lpm, and the measuring range of particle diameters is from 11 to 1100 nm. The particle number and mass size distributions are calculated from the data recorded and multiplied by the dilution ratio of the exhaust gas. The mean value of particle number and mass size distribution will be the average of three consecutively measured numbers.

As the exhaust gas flows through the exhaust pipe and the aftertreatment system from the diesel engine, there are the nucleation of particle inception, the surface growth of very small particles, and the coalescence and agglomeration of small particles.[33] These formation processes of particulates not only depend on the working conditions of the diesel engine but also are determined by the temperature, the pressure, and the gas component of the exhaust gas in the exhaust pipe. Therefore, in the current study, the number size distribution, mass size distribution and total mass concentration of particulates, and gas components at from P1 to P8 measuring points are measured and they are used to analyze the evolution features of PM emission under different operation conditions.

2.3 | Uncertainty analysis of experimental results

The uncertainties of the experiment measurements are mainly dependent on the experimental conditions and the measurement instruments. The specifications of the measurement instruments used in the experiment have been described in detail in literature 22. In the current study, for the purpose of completeness, they are listed in Table S1.

An uncertainty analysis could be performed for the experimental data using the propagation of error method described by Moffat and Giechaskie et al[34,35] The uncertainty analysis processes are described in Table S2.

2.4 | Energy efficiency analysis

In order to make an energy efficiency comparison under different operating conditions, the specific energy consumption β is defined the Equation (1) according to the idea of reference.[36]

$$\beta = \frac{\dot{m}_g c_{p,g}(T_s - T_g)}{\dot{H}_f} \times 100\% \tag{1}$$

where $\dot{m}_g$ is the mass flow rate [g/s], $c_{p,g}$ is the specific heat of gas at constant pressure [J/kg K], T_s is the average temperature of substrate in DPF [K], T_g is the temperature of exhaust gas at inlet [K], and $\dot{H}_f$ is the external supplemental energy [W].

The critical energy efficiency η_c is defined the Equation (2) according to reference 16.

$$\eta_c = \frac{\Delta\dot{E}_a}{\Delta\dot{E}_{a+}\Delta\dot{E}_{\text{sup}}} \times 100\% \tag{2}$$

where $\Delta\dot{E}_a$ is the energy consumed by the diesel engine under the critical threshold gas condition, and $\Delta\dot{E}_{\text{sup}}$ is the external supplemental energy required to achieve critical threshold gas property.

In the long-running operations under PRF operating conditions, there are not the accumulation of ashes in the filter as we observe the section of DPF, as shown in Figure S1. This further validated the ash accumulated in the filter could be blown away by reverse flow under PRF operating conditions. Therefore, the PM filter efficiency α_{PM} is defined the Equation (3).

$$\alpha_{\text{PM}} = \frac{c_{8\text{PM}}}{c_{2\text{PM}}} \tag{3}$$

where $c_{2\text{PM}}$ and $c_{8\text{PM}}$ are, respectively, the mean concentrations of PM at P2 and P8 measuring points.

The CO conversion rate α_{CO} is defined the Equation (4).

$$\alpha_{CO} = \frac{c_{8CO}}{c_{2CO}} \quad (4)$$

where c_{2CO} and c_{8CO} are, respectively, the mean concentrations of CO at P2 and P8 measuring points.

3 | RESULTS AND DISCUSSIONS

3.1 | Characteristics of unidirectional flow

Figure 3 shows the particle size distribution at P1, P2, and P7 measuring points as the exhaust gas flows the main line and q_v is 260 m^3/h under unidirectional operation condition. Left longitudinal coordinate is particle number concentration while right longitudinal coordinate is particle mass concentration in Figure 3.

The idealized diesel exhaust particle size distributions are that most of the particle mass exists in the accumulation mode in the 0.1-0.3 μm diameter range while the nuclei mode in the 0.005-0.05 μm diameter range contains 1%-20% of the particle mass and more than 90% of the particle number. In the current experiment, the exhaust gas flows from exhaust port to P1 through an exhaust pipe, the temperature of the exhaust gas at P1 drops to 120°C, and most of nuclei mode particles have been accumulated into mode particles through coalescence and agglomeration at P1. Therefore, the particle number size distribution is a bimodal curve which higher peak locates at a particle size of 190 nm and lower peak locates at a particle size of 349 nm. The particle number size is mainly distributed within 75-398 nm. The particle mass size distribution is also a bimodal curve which lower peak locates at a particle size of 243 nm and higher peak locates at a particle size of 349 nm. The particle mass size is also mainly distributed within 75-398 nm. Both number and mass sizes of particulates in

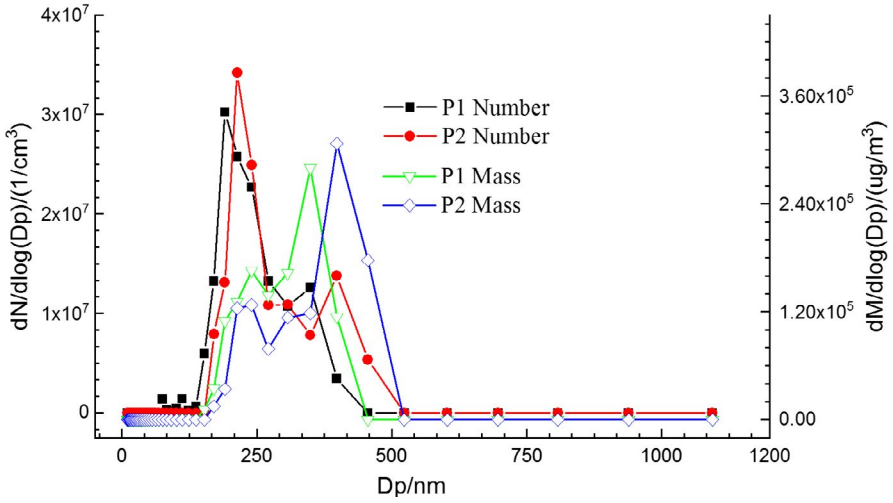

(A) Size distribution of PM at P1 and P2

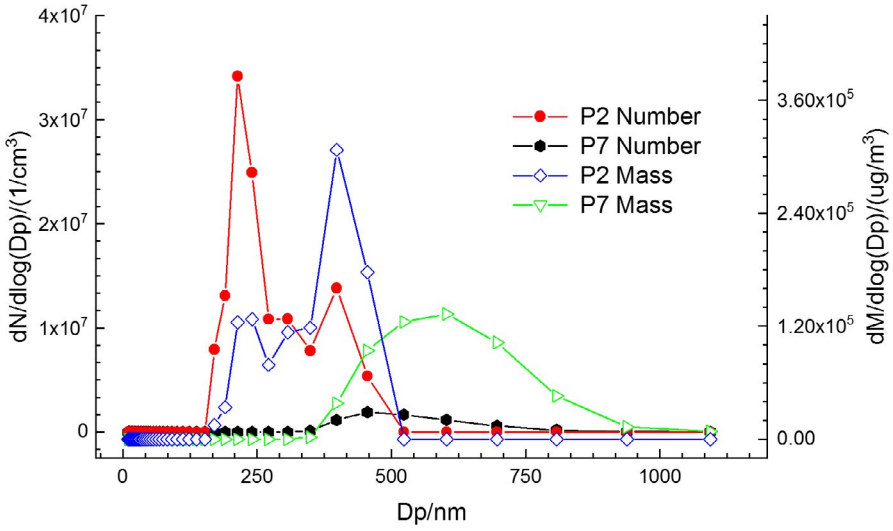

(B) Size distribution of PM at P2 and P7

FIGURE 3 Size distribution of PM at P1, P2, and P7 measuring points under unidirectional operation condition. A, Size distribution of PM at P1 and P2. B, Size distribution of PM at P2 and P7

the exhaust gas lie in the accumulation size range that is 50 nm < Dp < 1000 nm.

The temperature of the exhaust gas transitions from 120 to 80°C as the exhaust airflows directly from P1 to P2. Because the exhaust gas cools down, some of small size particles are converted into larger size particles through collision, coalescence, and agglomeration. It can be seen clearly from Figure 3A that both number and mass distribution ranges of particle size slightly become narrow and shift toward larger size particles, the position of two peaks is almost unchanged and the peak values increase at P2 compared with that at P1.

As the exhaust gas flows the main line, the mean components of O_2, CO, NO, NO_2, and PM in the exhaust gas at different measuring points under unidirectional operation condition are listed in Table 2. Total mass concentration of particle increases up from 140 to 197 mg/m^3 when the exhaust gas flows from P1 to P2 in Table 2.

When the exhaust gas is kept at about 80°C at P2, the temperature is lower than the light-off temperatures of PM, hydrocarbons, and CO. Only a small number of the hydrocarbons and CO are oxidized into H_2O and CO_2 under the action of bimetallic Pt/Pd catalytic agent and strong oxidant NO_2 in DOCs and DPF. Therefore, the mean component of CO and NO_2 decreases at P7 as listed in Table 2. As the exhaust gas flows through DPF, most of large PM are directly removed by filter. Therefore, total mass concentration of particle is reduced to 45.8 mg/m^3 from 197.1 mg/m^3 as exhaust gas flow from P2 to P7 in Table 2. But some of ultrafine particles can seep through the DPF and most of aromatic hydrocarbons as particulate precursor in exhaust gas can also be carried through the DPF. As a result, new particles are formed from the aromatic hydrocarbons through nucleation while the ultrafine particles are agglomerated into larger particles in second DOC under the cooling condition. Furthermore, the particle size distribution shifts to large size compared with that at P2 and the range of particle number and mass size distribution is mainly within 349-1100 nm at P7, as illustrated in Figure 3B. These further illustrate that the PMs detected are formed from the agglomeration of ultrafine particles and is belong to second particles. Thus, it can be seen, as the temperature is lower than the light-off threshold of combustible gas in the exhaust gas, the aftertreatment system can only remove the PM existed in the exhaust gas and cannot restrain the formation of second particles in atmospheric environment, under the low-temperature condition of unidirectional flow.

TABLE 2 Components of exhaust gas at various measuring point

Measuring Point	O_2/%	CO/ ppm	NO/ ppm	NO_2/ ppm	PM/mg/ m^3
P1	18.0	226.9	162.0	124.0	140.4
P2	17.9	226.7	169.0	119.0	197.1
P3	17.9	221.8	173.7	114.3	265.3
P7	17.8	171.92	178	105.0	45.8

3.2 | Influence of temperature distribution

Figure 4 shows the symmetrical temperature distribution curves during a reciprocating flow cycle as q_v is 260 m^3/h, fuel supplement is 0.16 m^3/h of C_3H_8 at the inlet, the temperature at P2 is 80°C, and T_c is 50 s. Figure 5 shows the asymmetrical temperature distribution curves during a reciprocating flow cycle under the same conditions as that in Figure 4. The mean components of O_2, CO, NO, NO_2, and PM in the exhaust gas at P2 in the two cases of symmetrical and asymmetrical temperature distribution are same as that in Table 2. For the two cases, utilizing a small amount of external fuel, the combined effects of the reversal flow, exothermic reaction, and solid heat retention result in a temperature distribution which exists a high-temperature region in the middle region and has high-temperature gradients on both sides in the aftertreatment system as shown in Figures 4 and 5.

As the initial high temperature is located in DPF, the symmetrical temperature distribution will be formed in the aftertreatment system under quasisteady states with PRF operation. The symmetrical temperature distribution is a parabola profile that the DPF is always kept at higher temperature and each DOC has a temperature gradient as is shown in Figure 4. The processes of alternately storing and releasing heat result in the periodic fluctuation of the temperature in the same location with PRF operation as is shown in Figure S2. The dividing point between endothermic regions and exothermic regions during the forward and backward flow is located in the same position, that is about $X = 0$ mm. From another perspective, during a forward flow operation the thermal wave propagates downstream and conversely for a backward flow operation, both following the directions of the exhaust gas flow. Thus, temperature distribution profile shifts toward the rear of the system during every half-cycle as shown in Figure 4A,B.

As the initial high temperature is located in left DOC or right DOC, the heat transfer between DOC and DPF is not achieved by heat conduction due to the existence of the space between them. The exothermic reaction as well as storing heat and releasing heat of the substrate could only been maintained in near initial high-temperature region during PRF operation. Therefore, an asymmetrical temperature distribution will be formed in the aftertreatment system under quasisteady states during PRF operation. An asymmetrical temperature distribution is formed because the initial high temperature is located in left DOC, as is shown in Figure 5. The asymmetrical temperature distribution is a trapezoidal profile which exists

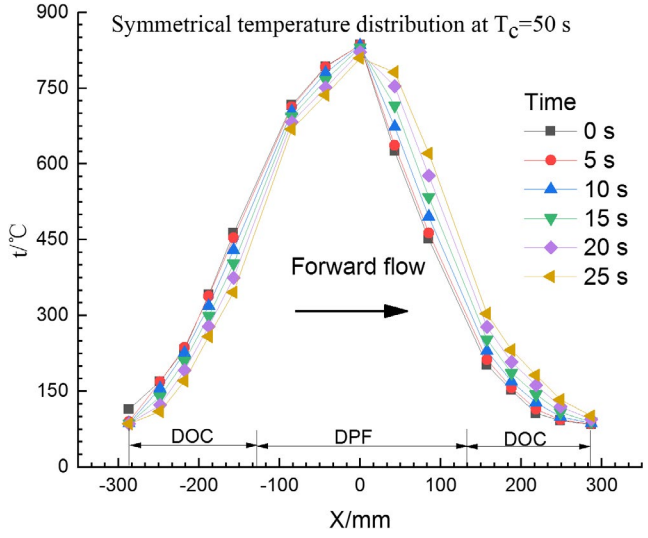

(A) Forward flow

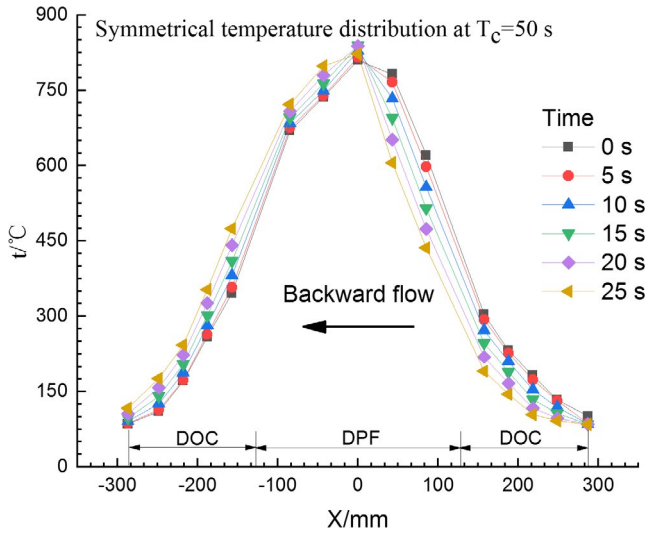

(B) Backward flow

FIGURE 4 Symmetrical temperature distribution profiles during 50-s cycle. A, Forward flow. B, Backward flow

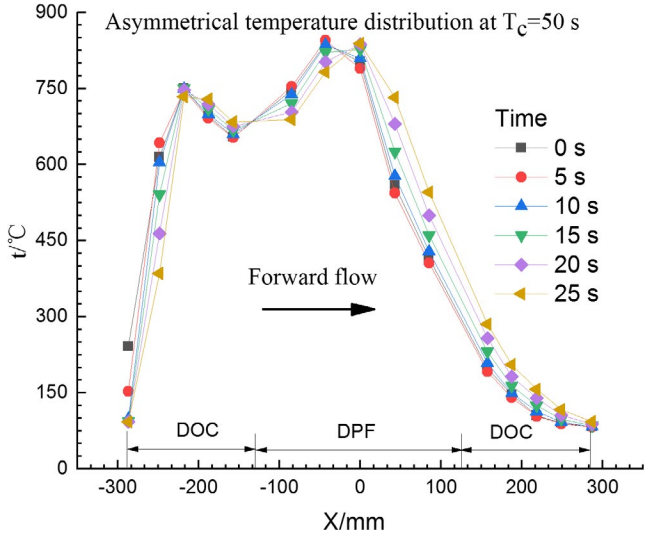

(A) Forward flow

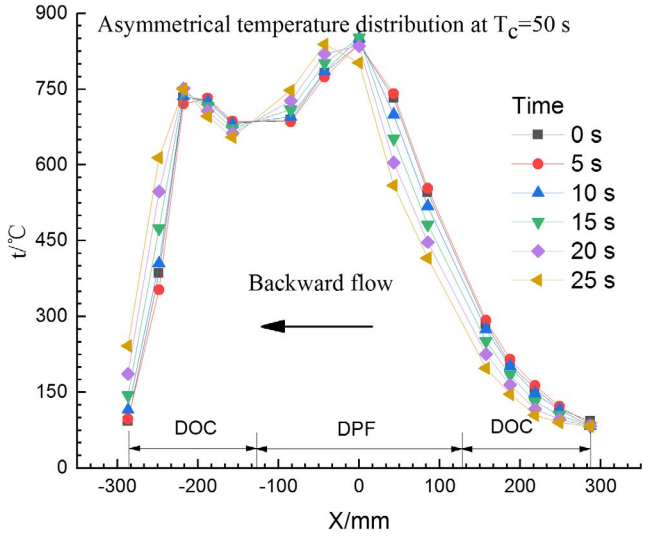

(B) Backward flow

FIGURE 5 Asymmetrical temperature distribution profiles during 50-s cycle. A, Forward flow. B, Backward flow

TABLE 3 α_{CO}, α_{PM}, and β for symmetrical and asymmetrical temperature distribution

State	α_{CO}	α_{PM}	β
Symmetry	93.96%	92.38%	124.22%
Asymmetric	91.57%	80.77%	122.49%

a high-temperature region within $-218\ \text{mm} \le X \le 45\ \text{mm}$ and has high-temperature gradients on both sides. The range of the high-temperature region in the case of asymmetrical temperature distribution is obviously larger than that in the case of symmetrical temperature distribution. The processes of alternately storing and releasing heat separately exist within four regions and the dividing points of the endothermic and exothermic regions separately locate at $X = -220$ mm, $X = -120$ mm, and $X = 10$ mm.

For the two cases, the CO conversion rate α_{CO}, the PM filter efficiency α_{PM}, and the specific energy consumption β are listed in Table 3. Based on above analysis, the symmetrical temperature distribution could form better mechanism of heat recuperation, and it has higher specific energy consumption β, as shown in Table 3.

Figure 6 shows the fluctuating curves of the total mass concentration of PM in the two cases of symmetrical and asymmetrical temperature distributions as $T_c = 50$ s. For symmetrical temperature distribution, the DPF is always kept at higher temperature than the lighting off temperature of soot oxidation. And each DOC has a temperature range from 80 to 450°C, most of the time the temperature is lower

than 400°C in the every half-cycle. Therefore, the chemical reaction equilibrium of NO_2 and NO is on the NO_2 side in DOCs most of the time in the every half-cycle. In upstream DOC, the hydrocarbons and CO in exhaust gas are oxidized into H_2O and CO_2 during every half-cycle.[37,38] Most of the particles attached on the walls of DPF passages are completely oxidized with the NO_2 catalytic action. The little incombustible residue as ash deposits on the walls. The HC and CO from incomplete oxidation conversion of soot are further oxidized into H_2O and CO_2 in downstream DOC. As switching to next a half-cycle from a half-cycle, the flow resided in the aftertreatment system carries PM suspended and flows reversely out. This includes the flow pipelines, the DOC channels, and the inlet passages of DPF at the end of the previous half-cycle before switching to next a half-cycle. The ashes deposited on the walls are also blown away the walls and carried out the aftertreatment system by the reverse flow. Therefore, as switching to next a half-cycle, the PM content rapidly increases to a peak value and then rapidly decreases. The content of PM periodically fluctuates, and the fluctuating amplitude is nearly equal for symmetrical temperature distribution, as shown in Figure 6A.

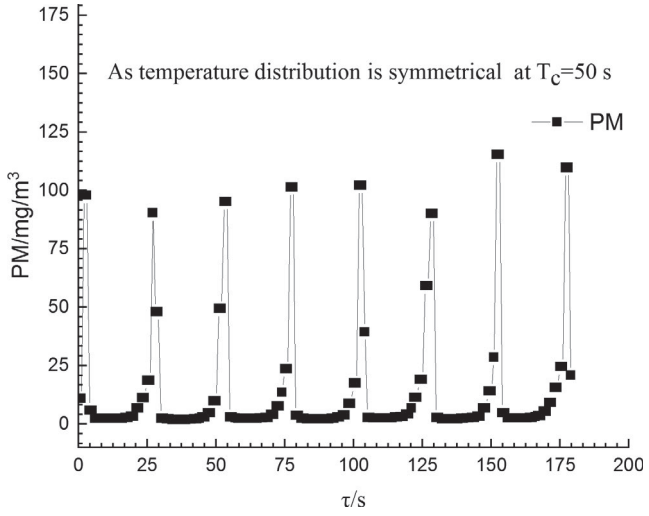

(A) Under symmetrical temperature condition

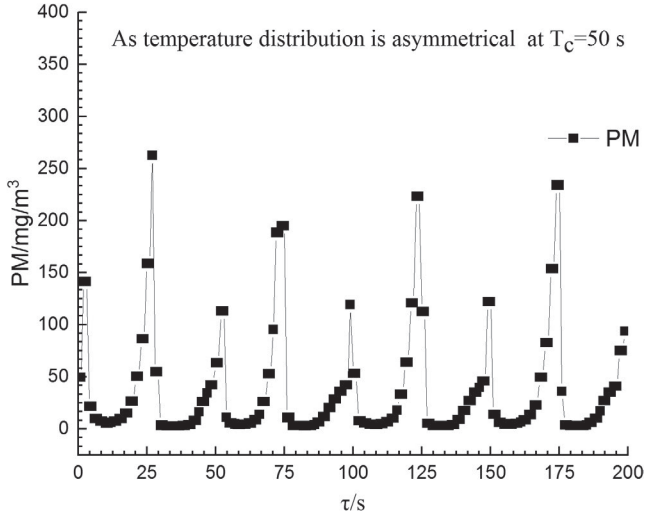

(B) Under asymmetrical temperature condition

FIGURE 6 Total mass concentration of PM at P7 for $T_c = 50$ s. A, Under symmetrical temperature condition. B, Under asymmetrical temperature condition

For asymmetrical temperature distribution, the DPF is also always kept at higher temperature than the lighting off temperature of soot oxidation. But temperature is in a range from 80 to 845°C, the temperature in the part region is higher than the 550°C in left DOC. Therefore, the chemical reaction equilibrium of NO_2 and NO is on the NO side in left DOC. The temperature is in a range from 80 to 300°C, most of the time the temperature is lower than 200°C in the every half-cycle in right DOC. Most of the time the conversion from NO to NO_2 could not been achieved at the temperature lower than 200°C in right DOC. Most of soot particles attached on the internal walls of the DPF are oxidized with O_2 alone and without the NO_2 catalytic action during every half-cycle. A small amount of particles incompletely oxidized deposit and reside on the internal walls of the DPF during every half-cycle. Every time switching to next a half-cycle, the flow resided in the aftertreatment system reversely flows out the

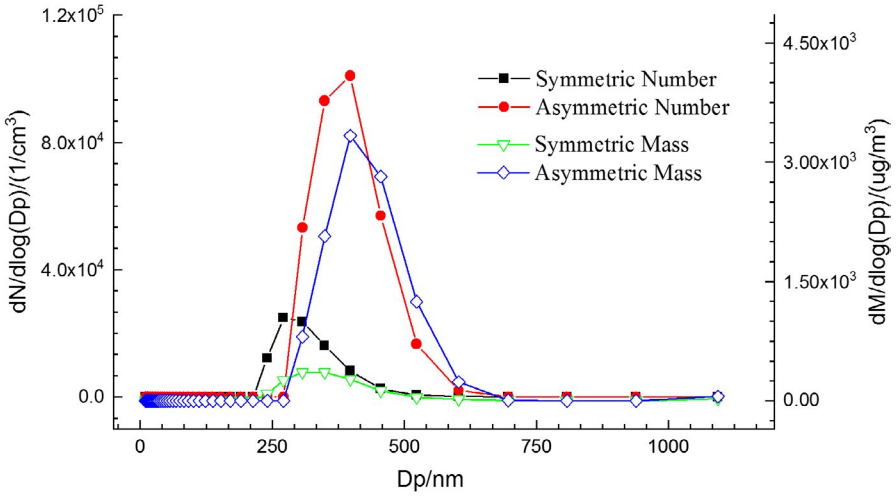

FIGURE 7 Size distribution of PM at P8 for symmetrical and asymmetrical temperature distribution

system. Subsequently, the residual particles deposited on the walls of the DPF during the previous half-cycle are stirred and gradually carried out by the reverse flow during the half-cycle. Therefore, for asymmetrical temperature distribution, as following the flow direction switch the PM content periodically fluctuates is same as that of symmetrical temperature distribution, but the fluctuating amplitude is different between forward flow cycle and backward flow cycle and every fluctuating amplitude is higher than that of symmetrical temperature distribution, as shown in Figure 6B.

Figure 7 shows the distribution curves of the particle size at P8 in the two cases of symmetrical and asymmetrical temperature distributions as $T_c = 50$ s. The mean components of O_2, CO, NO, NO_2, and PM in the exhaust gas at P8 in the two cases of symmetrical and asymmetrical temperature distribution are listed in Table 4.

For symmetrical temperature distribution, most of soot particles attached are oxidized and the continuous regeneration is realized in the DPF. Most of aromatic hydrocarbons as particulate precursor in the exhaust gas is also catalytically oxidized in the DOCs. The formation of second particles from nucleation, coalescence, and agglomeration can be effectively restrained. The particles escaped are mainly from the reverse flow resided in the aftertreatment system as switching to next a half-cycle from a half-cycle. Therefore, compared with the size distribution at P2 in Figure 3, the peak value of particle number is reduced by three orders of magnitude, while the peak value of particle mass is reduced by two orders of magnitude at P8 as is shown in Figure 7. The ranges of particle size distribution obviously narrow and shift toward smaller size particles. Total mass concentration of particle changes from 197.1 to 15 mg/m^3 as the exhaust gas flow from P2 to P8 across the aftertreatment system as listed in Tables 2 and 4.

According to the characteristics of asymmetrical temperature distribution, the particles deposited on the internal walls could not be completely oxidized in the system. The particles escaped are not only from the reverse flow resided in the aftertreatment system but also from the particles deposited on the internal walls. Therefore, compared with the symmetrical temperature distribution in Figure 7, the peak values of particle number and mass obviously increase, the ranges of particle size distribution widen and shift toward larger size particles. The PM filter efficiency α_{PM} decreases compared with the symmetrical temperature distribution, as shown in Table 3. Total mass concentration of particle changes from 197.1 to 38 mg/m^3 as the exhaust gas flows from P2 to P8 through the aftertreatment system as listed in Tables 2 and 4.

TABLE 4 Components of exhaust gas at P8 for symmetrical and asymmetrical temperature distribution

State	O_2/%	CO/ ppm	NO/ ppm	NO_2/ ppm	PM/ mg/m^3
Symmetry	17.4	13.7	245.9	20.0	15.0
Asymmetric	17.7	19.1	207.7	5.0	37.9

For PRF operation, the downstream DOC can be used to oxidize HC and CO produced from incomplete oxidation conversion of soot during every half-cycle. Therefore, CO conversion rate is high and CO emission is also kept at low level in both cases, as listed in Tables 3 and 4.

It can be seen that the symmetrical temperature distribution conditions can not only sustain above "light-off" temperature region in DPF, but also maintain high-temperature gradients in two DOCs. Thus, the symmetrical temperature distribution not only can ensure the catalyst coating having the best performance but also can reduce thermal stress in DPF. Compared with the asymmetrical temperature distribution under the same conditions, the aftertreatment system formed the symmetrical temperature distribution has better performance of trapping particles and regeneration.

3.3 | Influence of reciprocating flow cycle

Figure 8 shows the symmetrical temperature distribution profiles in the aftertreatment system during forward half-cycles as q_v is 260 m^3/h, fuel supplement is 0.16 m^3/h of C_3H_8 at the inlet, the temperature at P2 is 80°C, and T_c is 50 s, 80 s and 100 s, respectively. As T_c is 50 s, 80 s and 100 s, respectively, the CO conversion rate α_{CO}, the PM filter efficiency α_{PM} and the specific energy consumption β are listed in Table 5.

For the case of every reciprocating flow cycle, the temperature distribution curve at the end of previous backward half-cycle is almost same as that at the beginning of the next forward half-cycle, as shown in Figure 4, Figure S3, and Figure S5. For the case of every reciprocating flow cycle, the heat released heat solid substrate and forms thermal wave in DOCs and DPF after the chemical reactions are lighted-off at the beginning of every half-cycle. Subsequently, the thermal wave propagates downstream during the half-cycle. The thermal wave propagates

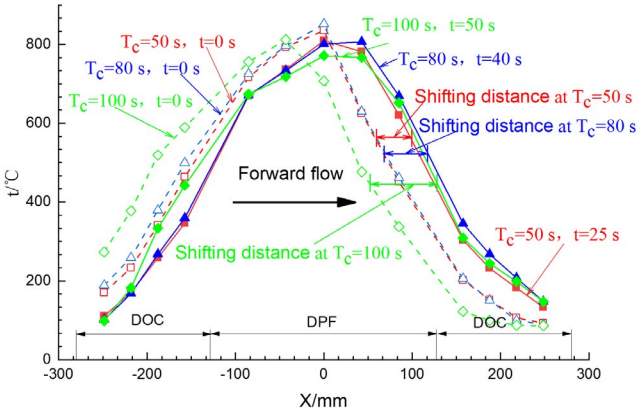

FIGURE 8 Temperature profiles as $T_c = 50$, 80, and 100 s

TABLE 5 α_{CO}, α_{PM}, and β for T_c = 50, 80, and 100 s

Symmetric cycle	α_{CO}	α_{PM}	β
50 s	93.96%	92.38%	124.22%
80 s	88.53%	88.93%	124.19%
100 s	83.41%	88.64%	117.69%

T_c = 80 s, and as shown in Figure 8. The specific energy consumption β decreases significantly, as shown in Table 5.

Figure 9 shows the distribution curves of the particle size at P8 as T_c is 50 s, 80 s, and 100 s, respectively. Left longitudinal coordinate is particle number concentration while right longitudinal coordinate is particle mass concentration in

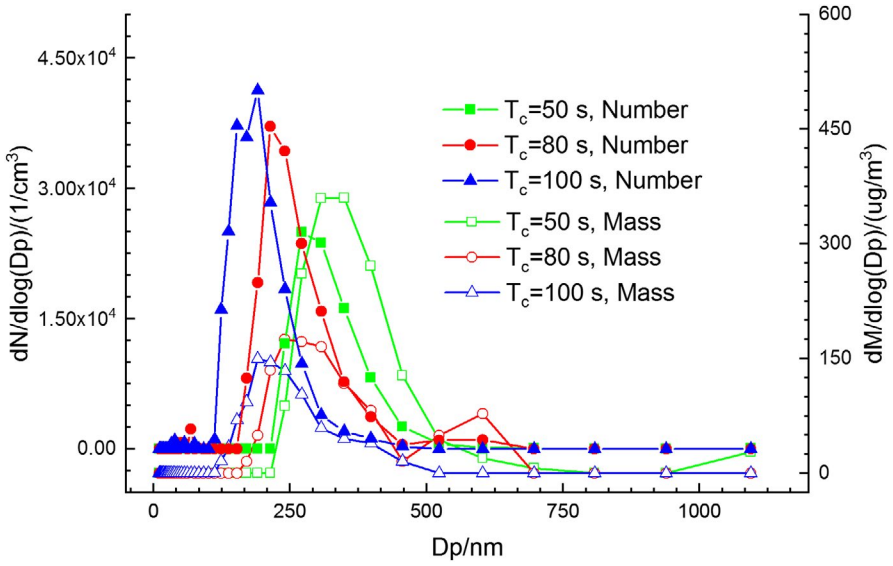

FIGURE 9 Size distribution of PM at P8 for T_c = 50, 80, and 100 s

downstream nearer to the outlet of downstream DOC, the temperature at the outlet of downstream DOC becomes higher, and the heat loss is more during the half-cycle. Therefore, the temperature in the high-temperature region gradually decreases along with temperature distribution profile shifting toward downstream during the half-cycle, as shown in Figure 4, Figure 8, Figure S3, and Figure S5.

With T_c increasing, because the time of thermal wave propagation downstream increases during a half-cycle, the moving distance toward downstream of the temperature distribution profile increases during the half-cycle and the high-temperature zone in the profile slightly becomes wider. As T_c increases up to 80 s from 50 s, the temperature of each DOC outlet at the end of every half-cycle slightly increases corresponding to the time increases in thermal wave propagation downstream as shown in Figure 8. Therefore, the heat loss increases slightly comparing with that at T_c = 50 s, and the specific energy consumption β changes little comparing with that at T_c = 50 s, as shown in Table 5. As T_c increases up to 100 s from 80 s, the temperature of left DOC outlet at the end of backward half-cycle significantly increases corresponding to the time increases in thermal wave propagation downstream, and the fluctuating amplitudes of temperature increase in the same location, as shown in Figure S4, Figure S5, Figure S6, and Figure S7. Therefore, the heat loss increases and the temperature in high-temperature region of the system at T_c = 100 s decreases comparing with that at Figure 9. As T_c is 50 s, 80 s, and 100 s, respectively, the mean components of O_2, CO, NO, NO_2, and PM in the exhaust gas at P8 are listed in Table 6.

Temperature in central zone of DPF is always kept at higher temperature than the lighting off temperature of soot oxidation in all three cases of T_c = 50 s, 80 s, and 100s, even if the temperature fluctuates during every half-cycle. Therefore, the oxidation conversation rate of soot particles captured in DPF almost is not affected by T_c increasing. Nevertheless, because the time that downstream DOC is kept at low temperature increases during a half-cycle, and thus, the oxidation conversation rates of aromatic hydrocarbons and CO decrease in the downstream DOC with T_c increase. Therefore, the amount of aromatic hydrocarbons escaped from the upstream of the system increase, and new relatively small PMs formed through nucleation increase in the downstream DOC under the cooling condition. This results into that the number of relatively small size particle increases with T_c increase as

TABLE 6 Components of exhaust gas at P8 for T_c = 50, 80, and 100 s

Symmetric cycle	O_2/%	CO/ ppm	NO/ ppm	NO_2/ ppm	PM/ mg/m^3
50 s	17.4	13.7	245.9	20.0	15.0
80 s	17.5	26.0	254.2	18.1	21.8
100 s	17.5	37.6	251.1	17.6	22.4

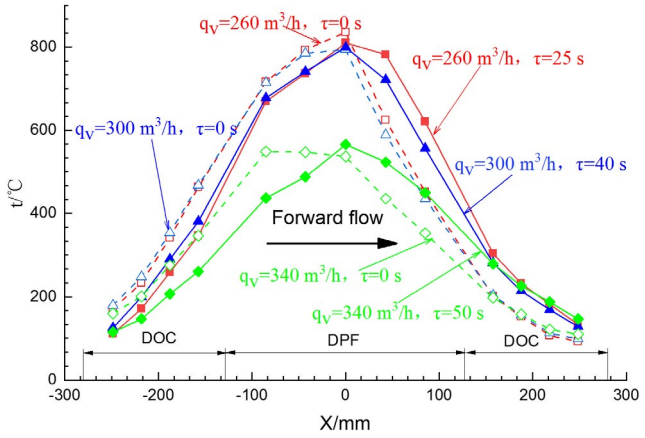

FIGURE 10 Temperature profiles as $T_c = 50$ s for $q_v = 260$, 300, and 340 m^3/h

TABLE 7 α_{CO}, α_{PM}, and β for different volume flow

Volume flow/m^3/h	α_{CO}	α_{PM}	β
260	93.96%	92.38%	124.22%
300	86.83%	87.82%	137.91%

shown in Figure 9. Conversely, with T_c increase the frequency of flow direction switching decreases, the mean number of the particles carried in the reverse flow has a certain amount of decrease. This results into that the number of relatively big size particle decreases with T_c increase as shown in Figure 9. The mass fraction of the relatively big size particle carried in the reverse flow is higher than the relatively small size particle formed through nucleation in the exhaust gas. Therefore, the mass of relatively big size particle decreases with T_c increase and particle mass size distribution region widens as shown in Figure 9. Based on the above reasons, the number peak value of particle size increases, the mass peak value of particle size decreases, and particle size distribution shifts toward less size particles at P8 with increasing T_c, as shown in Figure 9. Both CO conversion rate α_{CO} and the PM filter efficiency α_{PM} decrease with increasing T_c as listed in Table 5. Total mass concentration of particle emissions slightly increases, and the mean concentration of CO emissions increases at P8 with increasing T_c, as listed in Table 6.

3.4 | Influence of volume flow of exhaust gas

Figure 10 shows the symmetrical temperature profiles in the aftertreatment system during forward flow cycles as T_c is 50 s, fuel supplement is 0.16 m^3/h of C_3H_8 at the inlet, the temperature at P2 is 80°C, q_v is 260, 300, and 340 m^3/h, respectively. The CO conversion rate α_{CO}, the PM filter efficiency α_{PM}, and the specific energy consumption β are listed in Table 7. The mean concentrations of PM, NO, NO_2, and CO emission for different volume flow at P2 and P8 are listed in Tables 8 and 9, respectively.

Because the energy input is kept at 0.16 m^3/h of C_3H_8 and the convective heat transfer between exhaust gas and substrate is strengthened, the temperature of the exhaust gas flow through the system decreases with the increase of q_v. Therefore, the high-temperature zone in the system slightly narrows and temperature peak value slightly decreases from as q_v increases from 260 to 300 m^3/h as shown in Figure 10 and Figure S8. And the specific energy consumption β significantly increases, as shown in Table 7. If the volume flow of diesel engine exceeds a threshold, the energy input of 0.16 m^3/h C_3H_8 should not maintain stable operation of the system and the substrate temperature in DOCs and DPF should gradually reduce to the same as temperature of exhaust gas at P2. Therefore, it can be seen that the high-temperature zone obviously narrows and temperature peak value obviously decreases from as q_v increases from 300 to 340 m^3/h and q_v exceeds the threshold in Figure 10 and Figure S9. And the operation of the aftertreatment system could only lasted more than ten minutes. The threshold of the volume flow q_v could been further determined through experiments, and it is between 335 and 340 m^3/h. The critical energy efficiency η_c of the system is calculate according to the Equation (1), and it is equal to 96.61%.

With q_v increasing from 260 to 300 m^3/h, the high-temperature zone in the system slightly narrows and temperature peak value slightly decreases. Therefore, both CO conversion rate α_{CO} and the PM filter efficiency α_{PM} decrease with increasing q_v as listed in Table 7. The mean concentration of CO emission increases and the mean concentration of PM emission increases with the increase of q_v, as listed in Table 8 and Table 9.

4 | CONCLUSIONS

An experimental study is carried out to investigate the characteristics of the pollution emissions, the concentration and size distribution of PM emissions, and the temperature distribution of a PRF aftertreatment system applied in high power diesel engine. The effect of T_c and q_v of exhaust gas on the performance of the aftertreatment system is discussed in a systematic manner. The energy efficiency the aftertreatment

TABLE 8 Components of exhaust gas at P2 for different volume flow

Volume flow/m^3/h	O_2/%	CO/ ppm	NO/ ppm	NO_2/ ppm	PM/mg/ m^3
260	17.9	226.7	169.0	119.0	197.1
300	16.7	142.0	208.1	20.3	317.0

TABLE 9 Components of exhaust gas at P8 for different volume flow

Volume flow/m^3/h	O_2/%	CO/ ppm	NO/ ppm	NO_2/ ppm	PM/ mg/m^3
260	17.4	13.7	245.9	20.0	15.0
300	17.1	16.1	245.6	17.6	38.6

system is also analyzed. The main findings from the current work could be summarized as follows:

1. As the temperature of substrate is lower than the light-off threshold of combustible gas in the exhaust gas, the aftertreatment system could only remove the PM existed in the exhaust gas and could not restrain the formation of second particles in atmospheric environment, under the low-temperature condition of unidirectional flow.
2. The aftertreatment system has excellent performances of trapping particles and regeneration as the symmetrical temperature distribution is formed. The PM filter efficiency α_{PM} is 92%, and the specific energy consumption β is 124% for symmetrical temperature distribution.
3. The increase in T_c leads to the shifting of the temperature profile toward downstream, which would affect the particle number and mass size distribution as well as the characteristic of PM and CO emissions.
4. A certain increase in volume flow of exhaust gas could not alter the excellent temperature distribution characteristics.
5. The critical energy efficiency η_c of the system could reach 96.61%.

ACKNOWLEDGMENT

Our work in this paper has been supported in part by Coal Joint Fund of the National Natural Science Fund Committee of China—Shenhua Group Corporation Ltd. (NSFC Grant Nos. U1361111); the National Natural Science Foundation of China (NSFC Grant Nos. 5197022); Project supported by the Natural Science Foundation of Liaoning Province, China (Grant No. 2019-ZD-0164); Dalian Science and Technology Innovation Fund (Grant No. 2020JJ26SN065); and the Fundamental Research Funds for the Central Universities of China (Grant No. 3132019331).

ORCID

Yangbo Deng https://orcid.org/0000-0003-4909-0716

REFERENCES

1. Edouard D, Hammouri H, Zhou XG. Control of a reverse flow reactor for VOC combustion. *Chem Eng Sci*. 2005;60:1661-1672.
2. Karacan CÖ, Ruiz FA, Cotè M, Phipps S. Coal mine methane: a review of capture and utilization practices with benefits to mining safety and to greenhouse gas reduction. *Int J Coal Geol*. 2011;86:121-156.
3. Zagoruiko AN, Vanag SV. Reverse-flow reactor concept for combined SO_2 and co-oxidation in smelter off-gases. *Chem Eng J*. 2014;238:86-92.
4. Luzi CD, Martínez OM, Barreto GF. Autothermal reverse-flow reactors: design and comparison of valve-operated and rotary systems. *Chem Eng Sci*. 2016;148:170-181.
5. Luzi CD, Martínez OM, Barreto GF. Rotary reverse flow reactor vs. adiabatic reactor with regenerative preheating - design and comparison. *Chem Eng Sci*. 2017;166:246-261.
6. Marín P, Díez FV, Ordóñez S. Reverse flow reactors as sustainable devices for performing exothermic reactions: applications and engineering aspects. *Chem Eng Process*. 2019;135:175-189.
7. Gosiewski K, Pawlaczyk-Kurek A. Aerodynamic CFD simulations of experimental and industrial thermal flow reversal reactors. *Chem Eng J*. 2019;373:1367-1379.
8. Strots VO, Bunimovich GA, Matros YS, Zheng M, Mirosh EA. Novel Catalytic Converter for Natural Gas Powered Diesel Engines. SAE Technical Paper 980194; 1998.
9. Bunimovich GA, Strots VO, Matros YS, Mirosh EA. Reversed Flow Converter: Fundamentals of the Design. SAE Technical Paper, 1999-01-0459; 1999.
10. Matros YS, Bunimovich GA, Strots VO, Mirosh EA. Reversed flow converter for emission control after automotive engines. *Chem Eng Sci*. 1999;54:2889-2898.
11. Zheng M, Mirosh E, Klopp W, et al. Development of a Compact Reverse-Flow Catalytic Converter for Diesel Dual Fuel LEV. SAE Technical Paper, 1999-01-3558; 1999.
12. Konstandopoulos AG, Kostoglou M. Periodically reversed flow regeneration of diesel particulate traps. SAE technical paper, 1999-01-0469; 1999.
13. Konstandopoulos AG, Kostoglou M. Reciprocating flow regeneration of soot filters. *Combust Flame*. 2000;121:488-500.
14. Liu B, Checkel MD, Hayes RE, Zheng M, Mirosh E. Experimental and Modelling Study of Variable Cycle Time for a Reversing Flow Catalytic Converter for Natural Gas/Diesel Dual Fuel Engines. SAE technical paper, 2000-01-0213; 2000.
15. Liu B, Checkel MD, Hayes RE. Experimental study of a reverse flow catalytic converter for a dual fuel engine. *Can J Chem Eng*. 2001;79:491-506.
16. Zheng M, Reader GT. Energy efficiency analyses of active flow aftertreatment systems for lean burn internal combustion engines. *Energ Convers Manage*. 2004;45:2473-2493.
17. Zheng M, Reader GT, Wang D, et al. A Thermal Response Analysis on the Transient Performance of Active Diesel Aftertreatment. SAE technical paper 2005-01-3885; 2005.
18. Zheng M, Wang D, Reader GT. Boundary Layer Enhanced Thermal Recuperation for Diesel Particulate Filter Regeneration under a Periodic Flow Reversal Operation. SAE technical paper, 2005-01-0951; 2005.
19. Zheng M, Wang D, Reader GT, Wang M. Empirical and Theoretical Investigations of Active-flow Control on Diesel Engine Aftertreatment. SAE Technical Paper, 2006-01-0465; 2006.
20. Zheng M, Reader GT, Wang M. Investigation of active flow control on diesel engine aftertreatment. *J Propul Power*. 2008;24:376-383.
21. Zheng M, Banerjee S. Diesel oxidation catalyst and particulate filter modeling in active–flow configurations. *Appl Therm Eng*. 2009;29:3021-3035.
22. Deng Y, Wang X, Chen G, Wu H, Han Z, Li R. experimental study on a diesel particulate filter with reciprocating flow. *ACS Omega*. 2019;4:17098-17108.

23. Smith JD, Ruehl C, Burnitzki M, et al. Real-time particulate emissions rates from active and passive heavy-duty diesel particulate filter regeneration. *Sci Total Environ*. 2019;680:132-139.
24. Millo F, Vezza DS, Vlachos T, et al. Particle number and size emissions from a small displacement automotive diesel engine: bioderived vs conventional fossil fuels. *Ind Eng Chem Res*. 2012;51:7565-7572.
25. Lao CT, Akroyd J, Eaves N, et al. Modelling particle mass and particle number emissions during the active regeneration of diesel particulate filters. *Proc Combust Inst*. 2019;37:4831-4838.
26. Sarli VD, Benedetto AD. Operating map for regeneration of a catalytic diesel particulate filter. *Ind Eng Chem Res*. 2016;55:11052-11061.
27. Meng Z, Chen C, Li J, et al. Experimental study on regeneration performance and particle emission characteristics of DPF with different inlet transition sections lengths. *Fuel*. 2020;262:116487.
28. Meng Z, Chen C, Li J, et al. Particle emission characteristics of DPF regeneration from DPF regeneration bench and diesel engine bench measurements. *Fuel*. 2020;262:116589.
29. Fang J, Meng Z, Li J, et al. The effect of operating parameters on regeneration characteristics and particulate emission characteristics of diesel particulate filters. *Appl Therm Eng*. 2019;148:860-867.
30. Shi Y, Cai Y, Fan R, Cui Y, Chen Y, Ji L. Characterization of soot inside a diesel particulate filter during a nonthermal plasma promoted regeneration step. *Appl. Therm. Eng*. 2019;150:612-619.
31. Caroca JC, Millo F, Vezza D, et al. Detailed investigation on soot particle size distribution during DPF regeneration, using standard and bio-diesel fuels. *Ind Eng Chem Res*. 2011;50:2650-2658.
32. Tan P, Cao C, Hu Z, Lou D. A phenomenological model for particle number and size distributions of a diesel engine with a diesel oxidation catalyst. *Sci Total Environ*. 2019;672:536-550.
33. Xu G, Li M, Zhao Y. *Basic Theory of the Diesel Engine Particulate Emission*. Zhanjiang, China: Jiangsu University Press; 2017.
34. Moffat RJ. Describing the uncertainties in the experimental results. *Exp Therm Fluid Sci*. 1988;1:3-17.
35. Giechaskie B, Cresnoverh M, Jörg H, Bergmann A. Calibration and accuracy of a particle number measurement system. *Meas Sci Technol*. 2010;21:045102.
36. Zheng M, Banerjee S, Xu X, et al. Energy efficiency improvement of diesel aftertreatment with flow reversal and central fueling. Proceedings of the Internal Combustion Engine Division. ASME International, 2007 Fall Technical Conference. 2007, Charleston, South Carolina, USA. ICEF2007-1631.
37. Southward BWL, Basso S. An Investigation into the NO2-decoupling of Catalyst to Soot Contact and its Implications for Catalyzed DPF Performance. *SAE Int J Fuels Lubr*. 2009;1:239-251.
38. Southward BWL, Basso S, Pfeifer M. On the Development of Low PGM Content Direct Soot Combustion Catalysts for Diesel Particulate Filters. SAE Technical Paper, 2010-01-0558; 2010.

SUPPORTING INFORMATION

Additional supporting information may be found online in the Supporting Information section.

How to cite this article: Deng Y, Wang X, Li R, et al. Study on characteristics of particulate emission of diesel aftertreatment with reciprocating flow. *Energy Sci Eng*. 2021;00:1–13. https://doi.org/10.1002/ese3.882